Shallow sediment transport flow computation using time-varying sediment adaptation length

Jaan Hui Pu, Songdong Shao, Khalid Hussain and Yuefei Huang

Abstract

Based on the common approach, the adaptation length in sediment transport is normally estimated in the temporal independence. However, this approach might not be theoretically justified as the process of reaching of the sediment transport equilibrium stage is affected by the flow conditions in time, especially for those fast sediment moving flows, such as scour-hole developing flow. In this study, the 2D shallow water formulation together with a sediment continuity-concentration (SCC) model were applied to flow with mobile sediment boundary. A time-varying approach was proposed to determine the sediment transport adaptation length to treat the flow sediment erosion-deposition rate. The proposed computational model was based on the Finite Volume (FV) method. The Monotone Upwind Scheme of Conservative Laws (MUSCL)-Hancock scheme was used with the Harten Lax van Leer-contact (HLLC) approximate Riemann solver to discretize the FV model. In the flow applications of this paper, a highly discontinuous dam-break fast sediment transport flow was used to calibrate the proposed time-varying sediment adaptation length model. Then the calibrated model was further applied to two separate experimental sediment transport flow applications documented in literature, i.e. a highly concentrated sediment transport flow in a wide alluvial channel and a sediment aggradation flow. Good agreements with the experimental data were presented by the proposed model simulations. The tests prove that the proposed model, which was calibrated by the discontinuous dam-break bed scouring flow, also performed well to represent the rapid bed change and the steady sediment mobility conditions.

Keywords: Finite volume model; Harten Lax van Leer-contact solver; Monotonic upwind scheme; Sediment transport; Shallow water model; Time-varying sediment adaptation length

1 Introduction

Different numerical models have been proposed to simulate the sediment laden flows in various applications (e.g. Chen et al., 2007; Wu and Wang, 2007; Lin and Wang, 2006; Chen et al., 2011; Huai et al., 2011; and Lin et al., 2011). The sediment continuity (SC) model is one of the most common sediment transport models, which only considers the movement of sediment bed load capacity; hence it is also sometimes referred as the capacity model (Capart and Young, 1998). This model utilises the sediment volumetric transport rate to determine the sediment load and thus the bed elevations with regard to the temporal and spatial changes. In the more recent developments of the SC model, the non-equilibrium conditions caused by the bed load transient lag (Singh et al., 2004) and the higher order time-iteration accuracy in the alluvial flow simulation (Garcia-Martinez et al., 2006) were investigated. However, since the SC model only considers the sediment continuity equation, it could not be used to accurately represent the sediment transport flows with high suspended concentration.

Realising the shortcomings of the SC model, Armanini and Di Silvio (1988) initiated a set of sediment continuity-concentration (SCC) equations to improve the sediment transport representation by including the exchange effect of the sediment bed and suspended loads. Their model was solved in a 1D domain but it considered the non-equilibrium lag of the sediment transport. These equations were further tested by many researchers, i.e. by Valiani and Caleffi (2001) and

Wu and Wang (2007) for the case of dam-break sediment transport flow, and good correspondence between the numerical simulation and experimental data was observed.

Throughout the studies on sediment transport flow, a lot of different formulas for the sediment adaptation length L_A were proposed, as the characteristics of the sediment transport transition from non-equilibrium to equilibrium stage are hard to be uniformly predicted for different flow events. There were significantly different values of L_A being proposed in literature (refer to studies by Wu et al., 2004, and Wu, 2007). Nakagawa and Tsujimoto (1980), Phillips and Sutherland (1989) and Wu et al. (2000) used the average saltation step length of sediment in their experimental bed forms to be L_A in their numerical modelling studies. Bell and Sutherland (1983) found from their scour-hole development experiment on the bed degradation flow that L_A was time-dependent. Wu et al. (2004) also used the explicit time function on L_A to test on the degradation flow cases, although their results showed that there were no significant differences in between the time-dependent L_A with the time-independent ones.

In this paper, a summary of the research studies on the sediment adaptation length was given, and a time-varying sediment adaptation length approach to model L_A was proposed and tested with various experimental data from the literature. The combination of 2D shallow water and SCC models was used to simulate the sediment bed and suspended loads movement in a 2D depth averaged flow. The proposed model with the time-varying sediment adaptation length concept was first calibrated by a highly discontinuous dam-break fast sediment transport flow, and then the calibrated model was used to simulate the applications of a highly concentrated sediment transport flow in a wide alluvial channel and a sediment aggradation flow. For all tests, the experimental measurements from literature were used for validation. The model proved that the employed time-varying sediment adaptation length not only improved the numerical simulation of fast scour-hole development flow, like the discontinuous dam-break sediment transport flow, but it can also universally improve the simulation of the rapid bed change and the steady sediment mobility conditions in flow.

2 Governing equations

2.1 Shallow water model

The proposed model described in this paper was built using the sediment continuity-concentration model combined with the 2D shallow water flow equations. Equations (1) - (3) show the two-dimensional fully conservative shallow water equations, combined with the terms from the SCC model as suggested by Cao et al. (2004).

$$\frac{\partial \phi}{\partial t}+\frac{\partial \phi u}{\partial x}+\frac{\partial \phi v}{\partial y}=\frac{g}{1-\lambda}\left(e_s-d_s\right) \tag{1}$$

$$\frac{\partial \phi u}{\partial t}+\frac{\partial\left(\phi u^2+\phi^2/2\right)}{\partial x}+\frac{\partial \phi uv}{\partial y}=g\phi\left(S_{ox}-S_{fx}\right)-\frac{\phi^2\left(\rho_s-\rho_w\right)}{2\rho}\frac{\partial C}{\partial x}+\frac{ug\left(\rho_o-\rho\right)\left(d_s-e_s\right)}{\rho\left(1-\lambda\right)} \tag{2}$$

$$\frac{\partial \phi v}{\partial t}+\frac{\partial \phi uv}{\partial x}+\frac{\partial\left(\phi v^2+\phi^2/2\right)}{\partial y}=g\phi\left(S_{oy}-S_{fy}\right)-\frac{\phi^2\left(\rho_s-\rho_w\right)}{2\rho}\frac{\partial C}{\partial y}+\frac{vg\left(\rho_o-\rho\right)\left(d_s-e_s\right)}{\rho\left(1-\lambda\right)} \tag{3}$$

The variable ϕ refers to the geopotential, and is given by $\phi=g\cdot h$, where h is the water depth and g is the gravitational acceleration. u and v are the depth averaged flow velocities in the streamwise and lateral directions respectively. ρ_s and ρ_w are the density of sediment and water respectively, and $\rho=\rho_w\left(1-C\right)+\rho_s C$ and $\rho_o=\lambda\rho_w+\left(1-\lambda\right)\rho_s$. C is the flux-averaged volumetric sediment concentration of the total sediment load, and λ is the sediment bed porosity. x, y and t denote the spatial-longitudinal, spatial-transverse and time domains, respectively.

In the applications with a movable bed, a source term on the right hand side of equation (1) is implemented to capture the influence of erosion rate e_s and deposition rate d_s to the flow continuity. In equations (2) – (3), the second and third terms on the right hand side represent the spatial variations of sediment concentration and momentum transfer due to the process of sediment exchange between the water flow and erodible bed. Ferreirra and Leal (1998), Yang and Greimann (1999), Brufau et al. (2000) and more recently Xia et al. (2010) had suggested that the effects of those two terms in equations (2) – (3) are insignificant in most sediment flow applications. For more source terms modelling information on the momentum equation, one could also refer to Pu et al. (2012).

In equations (2) – (3), S_{ox} and S_{oy} are the bed slopes in the streamwise and lateral directions, respectively, and the friction slopes of the channel S_f are given by

$$S_{fx}=\frac{n^2u\sqrt{u^2+v^2}}{h^{4/3}}\text{, and} \tag{4}$$

$$S_{fy}=\frac{n^2v\sqrt{u^2+v^2}}{h^{4/3}} \tag{5}$$

where n is the Manning's friction coefficient.

2.2 Transport model of suspended and bed loads

The SCC equations are employed to represent the impact of sediment transport and these are represented as

$$\frac{\partial \phi C}{\partial t}+\frac{\partial \phi Cu}{\partial x}+\frac{\partial \phi Cv}{\partial y}=g\left(e_s-d_s\right) \tag{6}$$

$$\frac{\partial z_b}{\partial t}=\frac{1}{1-\lambda}\cdot\left(d_s-e_s\right) \tag{7}$$

where z_b is the bed elevation. The sediment erosion and deposition rates, e_s and d_s respectively, overhaul the source terms on the right hand side of equations (1), (6) and (7), and thus their evaluation holds a dominant role to determine the sediment load transport as well as the whole flow system.

3 Time-varying sediment adaptation length model

In the establishment of a sediment laden flow model, the sediment transport and bed deformation are usually modelled using the local flow condition with the assumption of low concentration regionally (refer to the studies by Cao et al., 2007 and 2011). However, this approach is overwhelmed with the inconsistency to represent the sediment transport especially at flow with the rapid bed deformation, as proven numerically by Cao et al. (2007) and experimentally by Needham and Hey (1991). Cao et al. (2007, 2011) have suggested a multiple time scale to numerically model the 1D fluvial and sediment transport processes in flow. However, this multiple time scale modelling involves further implementation of different time scales on each of the sediment transport parameters, and it could cause extra numerical complexities and costs.

As suggested previously by Cao et al. (2007, 2011), the time scale varying technique carries a significant role to improve the modelling of sediment transport process. Following this, in the current study we further investigate the possibility to represent the sediment transport process using more direct and numerically less-burdening time-varying approach. It is done by modifying the sediment adaptation length representation directly using the time-varying effect of sediment transport capacity. This approach is excluded from any major numerical scheme modifications, so it is not giving any extra computational cost to the numerical model. It is applied to the 2D shallow water model, and the formulation of this time-varying sediment adaptation length model is presented below.

To determine and implement the relationship of e_s and d_s, the model first suggested by Zhou and Lin (1998) and Valiani and Caleffi (2001) are utilised in this study. Compared with other works on the e_s and d_s relationship, the suggestion of Zhou and Lin (1998) and Valiani and Caleffi (2001) exhibits some outstanding characteristics by: 1) their inclusion of multiple sediment transport factors and parameters into the determination of e_s and d_s; and 2) their usage of empirically calibrated constants that had been kept as minimum as possible. Following Zhou and Lin (1998), Valiani and Caleffi (2001), and Wu (2007)

$$d_s-e_s=\frac{w_V\left(C-C_E\right)}{L_A} \tag{8}$$

where w_V is the sediment fall velocity; C_E is the equilibrium sediment concentration; subscript E refers to the equilibrium stage of sediment transport; and L_A is the dimensionless adaptation length for the sediment. In equation (8), when we separate the term on the right hand side, we will get $w_V C/L_A$ and $w_V C_E/L_A$, which represent the deposition and erosion rates, respectively, as suggested by Wu (2007). C_E is represented as

$$C_E=A\left[\frac{u^2+v^2}{\left(s_s-1\right)gd_{ms}}\right]^B \tag{9}$$

in which A and B are the coefficients for the sediment equilibrium concentration ($A=4.25E^{-4}$ and $B=1.5$ were suggested by the empirical tests of Valiani and Caleffi, 2001, using the dam-break sediment transport flow application). s_s is the specific density of the sediment and d_{ms} is the median diameter of the sediment.

The sediment adaptation length L_A was usually investigated by two interconnected approaches: 1) separated investigation using the suspended and bed load adaptation lengths; and 2) combined investigation of the total load adaptation length. Wu et al. (2004) and Wu (2007) outlined and compared the suspended and bed load adaptation lengths and used a comparison criterion to choose one of them to represent the total sediment adaptation length. By using the separated and combined suspended-bed load approaches studied by Fang et al. (2000, 2010), as well as Armanini and Di Silvio (1988) and Wu et al. (2000), respectively, a lot of calculation approaches had been initiated and designed for the sediment adaptation length, which contributed to better understanding of its characteristics.

Various different values were documented in literature for the sediment adaptation length, e.g. large values in Rahuel et al. (1989) and Fang (2003), and smaller values in Nakagawa and Tsujimoto (1980), Phillips and Sutherland (1989), Wu et al. (2000) and Liu and Shen (2010). This difference in the sediment adaptation length estimation is suggested by Wu (2007) to be caused by the different scale of experiments or field studies, where the former has much smaller sediment adaptation length than the latter. In terms of the methods to estimate it, a lot of studies used the time-independent saltation length of the flow bed condition to represent the sediment adaptation length. However, Bell and Sutherland (1983), Wu et al. (2004), and Wu (2007) conducted the tests of the sediment adaptation length in various time-functions on the bed degradation flows. The results of Bell and Sutherland (1983) showed that in the fast scour-hole development flow, the time-function was crucial to be used to estimate the sediment adaptation length.

Adapted from the equation originally proposed by Galappatti and Vreugdenhil (1985), which has also been further studied by Armanini and Di Silvio (1988), Valiani and Caleffi (2001) and Wu (2007), the dimensionless sediment adaptation length in equation (8) can be represented as

$$L_A = \alpha_A \left[\frac{L_R}{h} + \left(1 - \frac{L_R}{h}\right) \cdot \exp\left[-1.5 \left(\frac{L_R}{h} \right)^{-1/6} \frac{w_V}{u_s} \right] \right] \tag{10}$$

where u_s is the shear velocity of the flow; L_R is a reference level used as a comparison with the flow depth, which is suggested to be in the magnitude of median size of the sediment by Valiani and Caleffi (2001); and α_A is the adaptation coefficient of L_A.

There are a few scepticisms raised by the studies of Wu (2007) with regard to the current trend of estimating α_A and L_A in literature. First, in the highly eroded flows or the natural streams, bed load layer usually becomes thicker in time, so L_A in that case should be taking a non-constant reduction form in time. Second, it should not be assumed that the adaptation coefficients of erosion and deposition are the same until the equilibrium stage of sediment transportation is reached. Combining the afore-suggestions with the findings from Bell and Sutherland (1989), Wu et al. (2004) and Wu (2007), we propose an erosion-deposition relationship to the rapidly bed changing flow, e.g. scour-hole development flow. This relationship will renew equation (8) to

$$d_s - e_s = \frac{w_V C}{L_{A1}} - \frac{w_V C_E}{L_{A2}} \tag{11}$$

where

$$L_{A1} = \alpha_{A1} \left[\frac{L_R}{h} + \left(1 - \frac{L_R}{h}\right) \cdot \exp\left[-1.5 \left(\frac{L_R}{h} \right)^{-1/6} \frac{w_V}{u_s} \right] \right] \tag{12}$$

$$L_{A2} = \alpha_{A2} \left[\frac{L_R}{h} + \left(1 - \frac{L_R}{h}\right) \cdot \exp\left[-1.5 \left(\frac{L_R}{h} \right)^{-1/6} \frac{w_V}{u_s} \right] \right] \tag{13}$$

L_{A1} and α_{A1} correspond to the deposited sediment adaptation length; while L_{A2} and α_{A2} correspond to the entrained sediment adaptation length.

In the heavy scouring flow before reaching the sediment transport equilibrium stage, the eroded materials/substances will usually be accumulated intensely in a short period of time. At this stage, the erosion will be much more significant than the limited deposition that occurs. Hence, α_{A2} that is used to model the erosion needs to be in a time-function to describe the afore-mentioned pre-equilibrium sediment transport process. Studies of Lin (1984) and Spasojevic and Holly (1990) suggested that the natural logarithmic profile is suitable to be used to represent α_A, hence we implement a natural logarithmic time-dependency into α_{A2} that is effective up to the equilibrium sediment transport stage

$$\alpha_{A2} = \frac{\left(\frac{t_e - t}{t_e} \right)}{-Ln\left(\frac{t}{t_e} \right)}, \qquad \frac{t}{t_e} < 1 \tag{14}$$

where t_e is the equilibrium sediment transport time when $d_s = e_s$ occurs, and it is usually determined from the experimental condition. $L_{A1} = L_A$ is assigned for the sediment deposition modelling, where $\alpha_{A1} = 1$ holds since the deposition does not go through the same intense accumulation process before reaching equilibrium stage as the erosion. Using equation (14) into the relationship of deposition and erosion in equation (11) will make the erosion to increase boomingly at the start of the sediment transport. Then the erosion will decrease in the natural logarithmic form until the sediment transport equilibrium stage is reached. Before the reaching of natural equilibrium stage, $\alpha_{A2} > \alpha_{A1}$ always stands, and during this period, the natural logarithmic equation (14) creates a tendency of over-eroded flow to represent

the initial flow erosion condition. After getting passed the equilibrium stage, deposition and erosion adaptation lengths should be equal. So after the moment of equilibrium sediment transport, the model in equation (10) will be applied with $\alpha_A = \alpha_{A1}$. Different from most of the existing models, the proposed sediment adaptation length model facilitates the need of heavier erosion at the pre-equilibrium stage for any rapidly bed changing flows.

4 Numerical scheme

In this study, the numerical flux term was discretized using a Godunov-type Hancock scheme with a two-stage predictor-corrector time-stepping concept. The Godunov-type Hancock scheme was coupled with the Harten Lax van Leer-contact (HLLC) approximate Riemann solver for the Riemann data reconstruction process. The slope limiter method was used in the HLLC solver to ensure the space discretization scheme satisfying the flux-limiting property. The source term was modelled by a direct derivative approach as it has been known to cause less numerical instabilities as compared with the inviscid terms (Mingham and Causon, 2000 and Hu et al., 2006). By defining equations (1) – (3) and (6) – (7) into a single vector operation, we will get

$$\frac{\partial \mathbf{U}}{\partial t} + \nabla \cdot \mathbf{F} = \mathbf{S} \tag{15}$$

where

$$\mathbf{U} = \begin{bmatrix} \phi \\ \phi u \\ \phi v \\ \phi C \\ z_b \end{bmatrix}, \mathbf{F} = \begin{bmatrix} \phi \mathbf{Q} \\ \phi u \mathbf{Q} + \frac{\phi^2}{2}\mathbf{i} \\ \phi v \mathbf{Q} + \frac{\phi^2}{2} \\ \phi C \mathbf{Q} \\ 0 \end{bmatrix}, \mathbf{S} = \begin{bmatrix} \frac{g}{1-\lambda}(e_s - d_s) \\ g\phi\left(S_{ox} - S_{fx}\right) - \frac{\phi^2(\rho_s - \rho_w)}{2\rho}\frac{\partial C}{\partial x} + \frac{ug(\rho_o - \rho)(d_s - e_s)}{\rho(1-\lambda)} \\ g\phi\left(S_{oy} - S_{fy}\right) - \frac{\phi^2(\rho_s - \rho_w)}{2\rho}\frac{\partial C}{\partial y} + \frac{vg(\rho_o - \rho)(d_s - e_s)}{\rho(1-\lambda)} \\ g(e_s - d_s) \\ \frac{1}{(1-\lambda)}(d_s - e_s) \end{bmatrix} \tag{16}$$

In equations (15) and (16), $\mathbf{U}$, $\mathbf{F}$ and $\mathbf{S}$ represent vector forms for the flow conserved variables, numerical flux and source terms respectively; $\mathbf{Q}$ is the velocity vector defined by $\mathbf{Q} = u\mathbf{i} + v\mathbf{j}$; and ∇ is the gradient operator that can be expressed by $\nabla = \mathbf{i}\cdot\partial/\partial x + \mathbf{j}\cdot\partial/\partial y$. $\mathbf{i}$ and $\mathbf{j}$ are the unit vectors in streamwise and lateral directions, respectively.

4.1 HLLC approximate Riemann solver

The HLLC approximate Riemann solver used in this paper was suggested in Toro (1999) and has been further tested in Hu et al. (2006). In this solver, the numerical flux is determined by

$$\mathbf{F}^{hllc} = \begin{cases} \mathbf{F}_L & \text{for } 0 \le s_L \\ \mathbf{F}_L^* = \mathbf{F}_L + s_L\left(\mathbf{U}_L^* - \mathbf{U}_L\right) & \text{for } s_L \le 0 \le s_* \\ \mathbf{F}_R^* = \mathbf{F}_R + s_R\left(\mathbf{U}_R^* - \mathbf{U}_R\right) & \text{for } s_* \le 0 \le s_R \\ \mathbf{F}_R & \text{for } s_R \le 0 \end{cases} \tag{17}$$

and

$$\mathbf{U}_D^* = \left(\frac{s_D - u_D}{s_D - s_*}\right)\mathbf{U}^* \tag{18}$$

Subscripts L and R represent the left and right regions of the solution cell respectively; and superscript * represents the star region that separates the left and right regions. An extra wave speed s_* is employed by the HLLC solver in the star region for updating the numerical flux. The subscript D in equation (18) represents the direction of the parameters (left L or right R). The wave speeds are given by:

$$\begin{aligned} s_L &= \min\left[u_L - c_L,\ u_* - c_*\right] \\ s_* &= \frac{(u_L + u_R)}{2} + c_L - c_R = u_* \\ s_R &= \min\left[u_R + c_R,\ u_* + c_*\right] \end{aligned} \tag{19}$$

where c is the celerity wave ($c = \sqrt{gh}$), and in the * region, c^* is estimated as

$$c^* = \frac{(c_L + c_R)}{2} + \frac{(u_L - u_R)}{4} \tag{20}$$

In the shock capturing process, as utilised by the HLLC solver, the "dry" water wave front has to be resolved before obtaining a stable algorithm. In this study, further criteria as suggested by Toro (1999) are included to handle the water wave front condition on the left and right "dry" sides as follows

Left "Dry" Side Criteria: $s_L = u_R - 2c_R$, $s_* = s_L$, and $s_R = u_R + c_R$ (21)

Right "Dry" Side Criteria: $s_R = u_L + 2c_L$, $s_* = s_R$, and $s_L = u_L - c_L$ (22)

4.2 MUSCL–Hancock scheme

In the most primitive Godunov scheme, a constant piecewise linear approximation was used for the increments of $\mathbf{U}_L$ and $\mathbf{U}_R$ in time. This assumption has been shown to deflect the wave flux away from the actual wave solution while iterating through time. In this study, a more robust numerical wave reconstruction scheme, MUSCL scheme, was used, in which both $\mathbf{U}_L$ and $\mathbf{U}_R$ change linearly according to their adjacent cells (Toro, 1999). The MUSCL scheme gives a second order of accuracy to the proposed FV model, and it can be expressed as

$$\mathbf{U}^L_{i+1/2} = \mathbf{U}_i - \frac{\prod(k_i)\cdot\Delta\mathbf{U}_{i-1/2}}{2}, \text{ and, } \mathbf{U}^R_{i+1/2} = \mathbf{U}_{i+1} + \frac{\prod(k_{i+1})\cdot\Delta\mathbf{U}_{i+1/2}}{2} \quad (23)$$

where,
$$k_i = \frac{\Delta\mathbf{U}_{i+1/2}}{\Delta\mathbf{U}_{i-1/2}},\ k_{i+1} = \frac{\Delta\mathbf{U}_{i+3/2}}{\Delta\mathbf{U}_{i+1/2}},\ \Delta\mathbf{U}_{i+1/2} = \mathbf{U}_{i+1} - \mathbf{U}_i, \text{ and, } \Delta\mathbf{U}_{i-1/2} = \mathbf{U}_i - \mathbf{U}_{i-1} \quad (24)$$

In equations (23) – (24), $\prod$ is the slope limiter; i represents the space step; and k is the gradient of successive $\Delta\mathbf{U}$. The van Leer limiter was adopted, where $\prod = \left[k + |k|\right]/(1+k)$, as it was suggested to be the best limiter in the studies by Mingham and Causon (2000) and Hu et al. (2006).

A Hancock two-stage predictor-corrector scheme was utilised to update $\mathbf{U}$ in the time domain. This approach has the advantage of being stable and could achieve second order accuracy over the time domain. The combined predictor-corrector steps are given as

Predictor Step: $$\mathbf{U}_i^{N+1/2} = \mathbf{U}_i^N - \frac{\Delta t}{2\Omega_i}\left(\mathbf{F}^N_{i+1/2} - \mathbf{F}^N_{i-1/2}\right) \quad (25)$$

Corrector Step: $$\mathbf{U}_i^{N+1} = \mathbf{U}_i^N - \frac{\Delta t}{\Omega_i}\left(\mathbf{F}^{N+1/2}_{i+1/2} - \mathbf{F}^{N+1/2}_{i-1/2}\right) \quad (26)$$

where Ω is the cell volume; and N represents the time step.

A stability criterion, Courant-Friedrichs-Lewy criterion, was used to ensure Δt does not exceed its maximum allowable limit, as represented by

$$\Delta t \le C_{FL}\left[\frac{\Omega}{|\mathbf{Q}| + c\cdot|\boldsymbol{s}|}\right] \quad (27)$$

where $\boldsymbol{s} = (\boldsymbol{s}_x, \boldsymbol{s}_y)$ represents the resultant normal unit vector; $\boldsymbol{s}_x$ and $\boldsymbol{s}_y$ represent the normal unit vectors in streamwise and lateral directions respectively; and C_{FL} is the Courant number, which is limited to $0 < C_{FL} \le 1$. Smaller values of C_{FL} give more accurate and stable results, but at an increasing computational cost. $C_{FL} = 0.8$ is used in all the tests of this study.

4.3 Boundary and initial conditions

A double boundary condition is used for the FV model, where the two extra ghost-cells are utilised outside the computational space domain (Hu et al., 2006). Two kinds of boundary are considered, open and solid boundaries. For their corresponding boundary vectors $\boldsymbol{U}^{\boldsymbol{B}}$, it can be presented as $\boldsymbol{U}^{\boldsymbol{B}} = \left[\phi \quad \phi u \quad \phi v \quad \phi C \quad z\right]^T$ for the solid boundary and $\boldsymbol{U}^{\boldsymbol{B}} = \left[\phi \quad -\phi u \quad -\phi v \quad \phi C \quad z\right]^T$ for the open boundary. These boundary conditions were updated using

$$\mathbf{U}^{\boldsymbol{B}}_{m+1} = \mathbf{U}^{\boldsymbol{B}}_{m} \quad (28)$$

$$\mathbf{U}^{\boldsymbol{B}}_{m+2} = \mathbf{U}^{\boldsymbol{B}}_{m-1} \quad (29)$$

where m is the last space step in the computational boundary excluding the ghost cells.

5 Results and discussions

Three sediment flow applications were used to test the proposed numerical model. These applications were: 1) sediment transport induced by a dam break flow, 2) highly concentrated sediment transport in a wide alluvial channel flow, and 3) sediment aggradation flow. The simulation results were compared with the experimental data from the previous studies and good agreement between them was observed.

5.1 Dam-break flow in sediment transport channel

An experiment investigated by Capart and Young (1998) was simulated using the proposed model and the results are reported herein. A rectangular channel with dimensions of 12.0m in length and 0.2m in width was used in Capart and Young (1998) experimental test. The sediment had a size of 6.1mm, a density of 1048kg/m^3, and a fall velocity of 0.076m/s. The flow was initially set at rest, where it had an initial water depth of 10cm at the upstream, dry water depth at the downstream, and a layer of 6cm sediment at the bed throughout the channel from the upstream to downstream. The sluice gate, which was originally situated at 4m location from the upstream, was lifted completely and instantaneously at the start of the flow. The results of the water surface and bed elevation profiles around the dam breaking point are shown in Fig. 1, where the water surface was taken from the datum of the bed elevation. The SC modelling results from Capart and Young (1998), and the SCC modelling results from Wu and Wang (2007) are also plotted in the same figure for comparison.

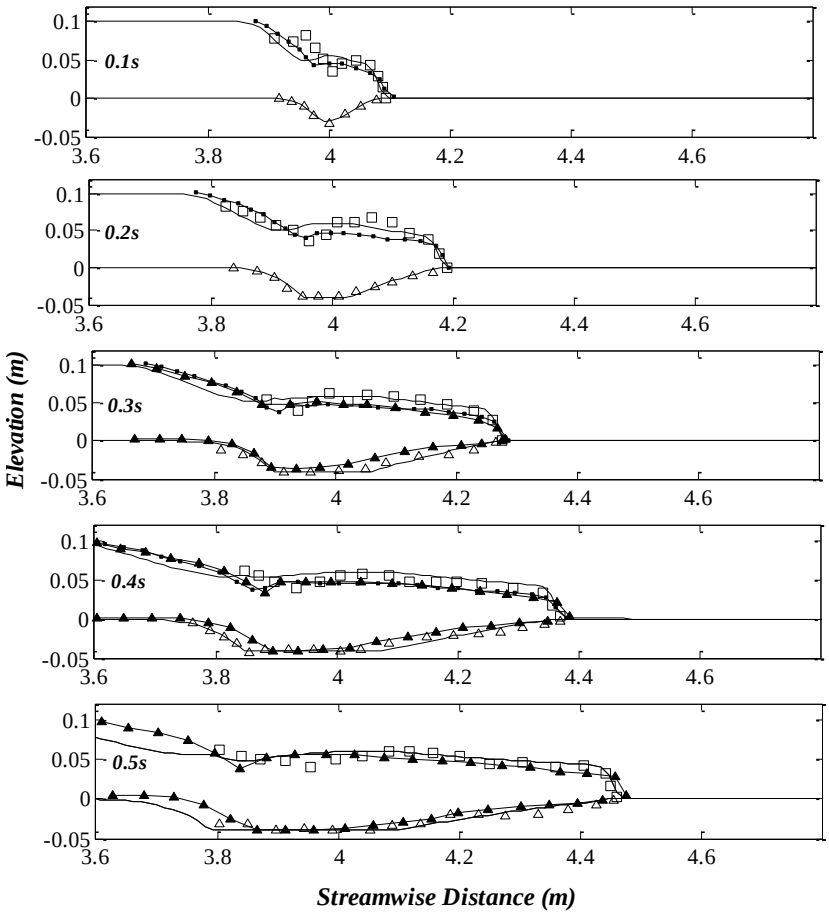

Fig. 1 Water surface and bed profiles comparisons – proposed model (solid line), Capart and Young (1998) model (line with dots), Wu and Wang (2007) model (line with triangles), measured water level (hollow squares) and measured bed level (hollow triangles)

Comparing the numerical and experimental results during the early stage of the dam break (at 0.1s), two hydraulic jumps in the water surface were observed in the experimental measurement, whereas the proposed model and Capart and Young (1998) model showed only one. This was believed to be caused by the excessive vertical wave momentum induced from the sluice-gate movement at the start of the experiment, which has not been accounted for by the proposed depth-averaged model or the Capart and Young's model. However in comparison, the proposed model showed a better capability to capture the water wave front location and magnitude than that of Capart and Young (1998). Besides, the scour hole created by the dam-break flow was also accurately simulated by the proposed model. After 0.2s of flow as shown in Fig. 1, the hydraulic jumps at the water surface propagated in two opposite directions – towards the upstream (in depression wave) and downstream (in bore wave) to flatten the wavy flow surface previously observed at 0.1s. At that instant, the proposed model predicted the measured water wave front more accurately compared with Capart and Young (1998) model. As for the bed profile measurement, it has also been well-predicted by the proposed model. At 0.3s, the proposed numerical model simulated a very close resemblance of the water surface wave to the experimental

measurement. Although the upstream depression wave from the dam location was slightly over-estimated, the bed scour was accurately modelled with a marginally small magnitude of under-erosion. Compared with the simulation results presented by Capart and Young (1998), and Wu and Wang (2007), the proposed model demonstrated significantly improved wave propagation prediction at the water wave front. The proposed model also showed better prediction of the bed profiles as compared with the over-deposited results by Wu and Wang (2007).

Fig. 1 also shows that the proposed model exhibited a high accuracy in resolving both the water wave and bed scour formed at 0.4s. Again the proposed model simulated the water wave front (both water wave shape and magnitude) more accurately than Capart and Young (1998), and Wu and Wang (2007) models, although its celerity propagation was slightly lower at the dam location compared with the measurements. At the bed, the proposed model simulated the erosion at the upstream location (from dam) more accurately than Wu and Wang (2007) model, and also captured the downstream deposition in a satisfactory manner. Also at 0.5s, the water wave front propagation and sediment bed evolution were also predicted slightly more accurately by the proposed model compared with Wu and Wang (2007) model.

In summary, both the crucial dam break flow information of water wave front and bed scour hole size have been well-predicted using the proposed model. Numerically, the proposed time-varying sediment adaptation length in the sediment transport model increased the modelling capability to capture the time-dependent dam-break flow bed evolutions compared with the commonly used time-constant approaches. To further investigate this, Fig. 2 is produced in which the time-varying sediment adaptation length simulations are compared with the results without using the time-varying sediment adaptation length. It is obvious that the time-varying approach reproduced closer the experimental measurements and improved the accuracy over the conventional model. The improvement was seen in the predictions of both the water wave front and the bed scour variations. Here it is noted that in this particular flow application, the main advantage of the time-varying formulation is to give an improved simulation on the sediment transport at the downstream of the dam location.

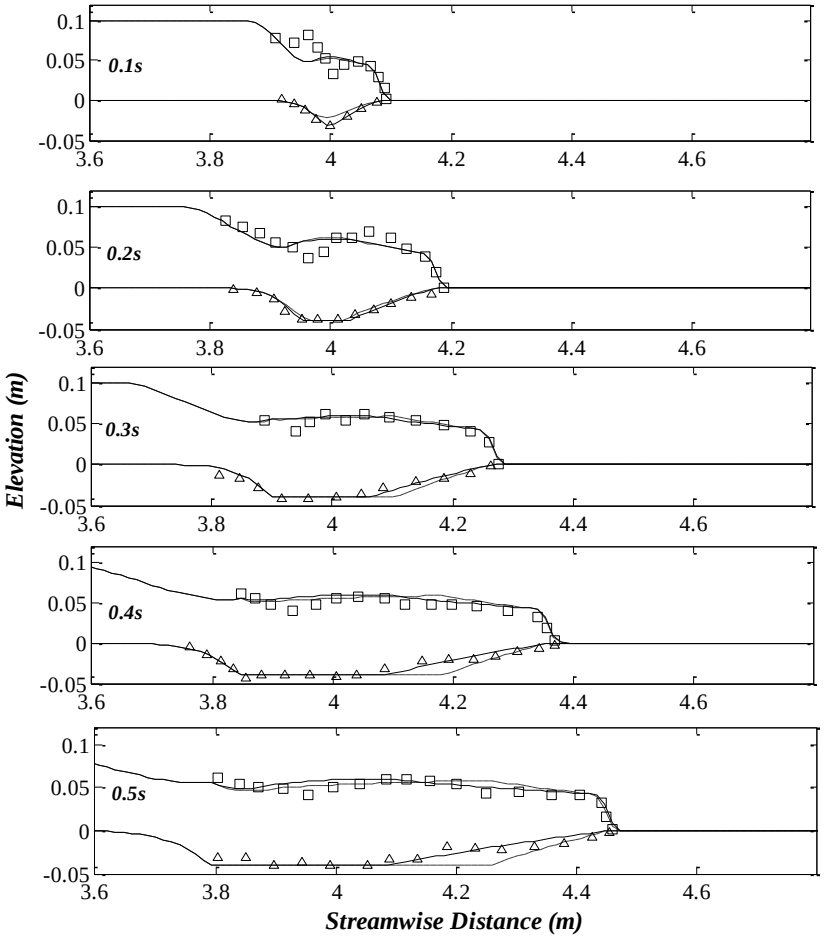

Fig. 2 Water surface and bed profiles comparisons – model with T.V.S.A.L.A. (solid line), model without T.V.S.A.L.A. (dashed line), measured water level (hollow squares) and measured bed level (hollow triangles) (T.V.S.A.L.A. stands for Time−Varying Sediment Adaptation Length Approach)

5.2 Highly concentrated flow in a wide alluvial channel

The data set reported by Wren et al. (2005) was selected for comparison with the proposed numerical model here. In the experiment, a rectangular flume with dimensions of 30m long and 1.2m wide was used with a fast moving backscatter acoustic device to measure the rapid sediment movement. Initially, the height of water and the thickness of sediment bed were set at 0.13m and 0.15m respectively. The initial flow velocity was set at 0.53m/s. The median size of the sediment used was 0.52mm and the bed had a porosity of 0.4. A Manning's coefficient of 0.02 was used to represent the bed roughness and the bed slope was 0.003.

The simulated water and sediment surfaces at 7s, 21s, 34s and 48s for the test are presented in Fig. 3. One can observe that at the simulation time of 7s, the water surface exhibited an undulating form, which has evolved into a more uniform flow later, as reflected by the Figs. 3(b) – 3(d), corresponding to 21s, 34s and 48s. It can be also noted that the upstream water movement experienced a heavy smearing effect. Most of the flow kinetic energy was used to create a scour area. At the same time, the flow eroded the bed sediment to produce a high suspended sediment concentration in the flow. As a result, the slow-moving flow generated a higher surface elevation upstream. When the flow propagated to the mid-stream of the channel, part of the suspended solid materials re-deposited as the bedload to form a sediment hump on the bed. This hump is not too distinguishable as it is flat and broad. Throughout the location of the hump, the sediment deposition is typically slow, at an average rate of 1.1mm/s during the first 7s; and this rate further decreased in time to an average of 0.7mm/s after 48s. At the downstream location, a strong erosion effect was observed, in which a big portion of the sediment bed was entrained through time. Over the time, the simulated water surface elevation increased, but with a reasonably small amount (increased by an average of 7.1% from 7s to 48s), due to the suspended solid materials being entrained into the flow. There are two noticeable developments of the sediment bed over time: (1) the enlargement of scour hole upstream; and (2) the increase of eroded area downstream. Both processes contributed to the drastic increase in the erosion rate and locally predominant suspended load in flow.

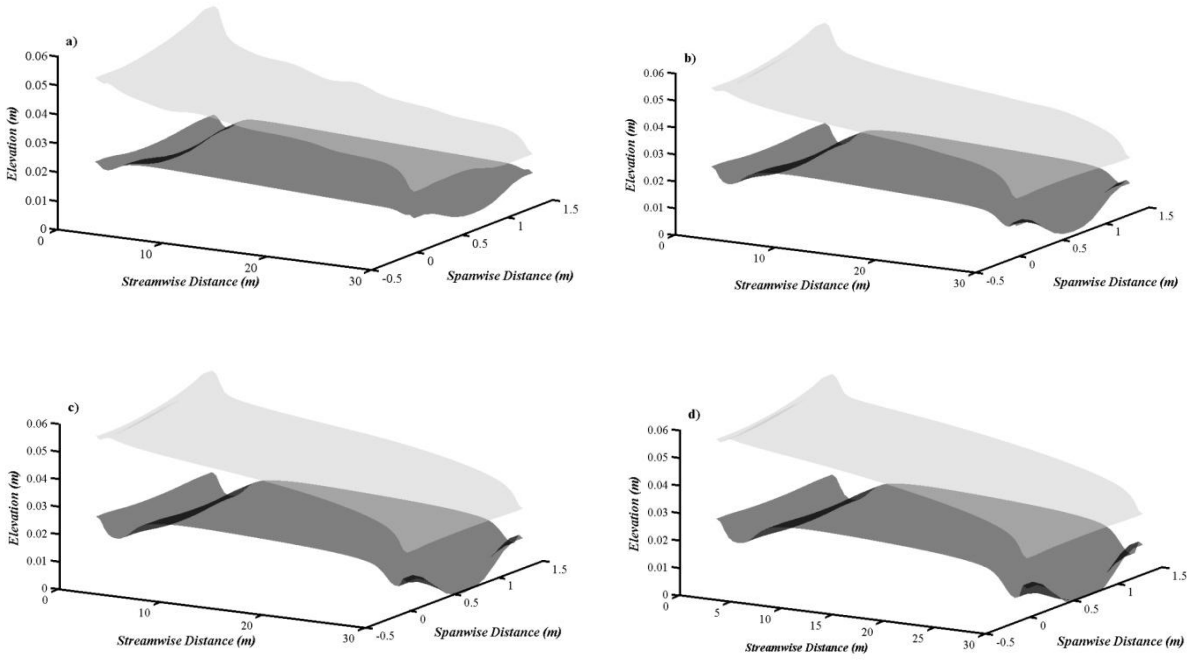

Fig. 3 Three dimensional water surface (grey surface) and bed form (dark surface) at a) 7s, b) 21s, c) 34s and d) 48s

The simulated sediment elevations as obtained by the proposed model at 7s, 21s, 34s and 48s at the downstream position of 23.6m are compared with the experimentally measured bed elevations in cross-sectional direction by Wren et al. (2005) in Fig. 4. In Wren's experiment, the bed surface elevations at different times were estimated from the sediment concentration profiles. Meanwhile, the computational results from the sediment transport model without the time-varying approach on the sediment adaptation length are also plotted in the figures for a comparison. Referring to Fig. 4(a) – (c), it can be observed that after 7s the predictions from both numerical models show relatively close correspondence with the experimental measurement of sediment depth, especially near to both sidewalls. However, the proposed model with a time-varying formulation has predicted a more accurate sediment depth result than that of the conventional sediment transport model after 48s in Fig. 4(d). Generally speaking, one could observe that both numerical models have predicted the experimental measurements from 7s to 34s with reasonably good agreement. However, as the

time progressed (at 48s), the proposed time-varying sediment adaptation length model provided a much better prediction to the experimental measurements.

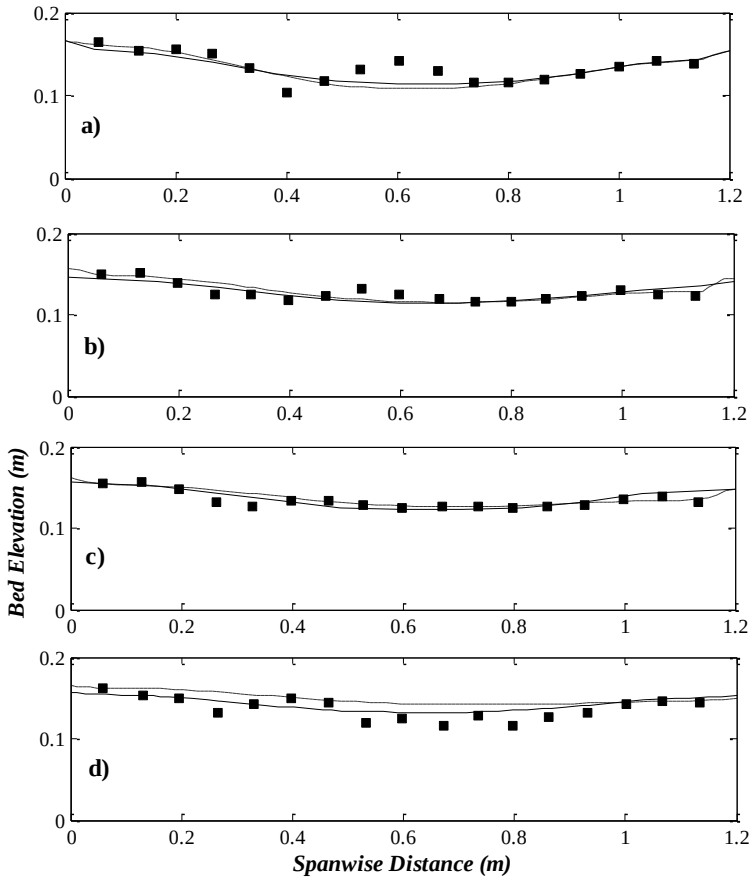

Fig. 4 Sediment bed spanwise elevation at a) 7s, b) 21s, c) 34s and d) 48s − model with T.V.S.A.L.A. (solid line), model without T.V.S.A.L.A. (dashed line) and bed measurements (squares)

At the onset of alluvial channel flow process, a sediment bed form 'dune' was formed at the mid-stream of the flow [refer to the measured profile at 7s in Fig. 4(a)]. Very slowly through time, this dune disappeared as it was re-eroded by the flow and deposited further downstream. It is possible that this dune was caused by the secondary current created in the recirculation direction from the slow motion flow at the sidewalls towards the fast motion main-stream at the mid-channel (see Nezu and Nagakawa, 1993, for detailed mathematical and experimental studies and explanations on the secondary current). The dune formed was highly unstable and likely to exchange its form in-between the bed and suspended loads in time. As expected, the secondary current and the subsequent sediment distribution patterns at the mid-section were not well-simulated by both numerical models, as those models did not take into account the formation of the secondary current.

5.3 Sediment aggradation flow

In this section, the experimental flow applications with the sediment aggradation process by Soni et al. (1980) are investigated numerically using the proposed time-varying sediment adaptation length model. Soni et al. (1980) experiments were conducted in a channel of 30m long and 0.2m wide. The Chezy coefficient C used in the applications was 29.69m$^{1/2}$/s and the sediment bed porosity λ was 0.40. The mean diameter of the sediment used was 0.32mm. Two separate experimental tests of Soni et al. (1980) were simulated by the proposed model and their full descriptions and conditions are presented in Table 1.

Table 1 Initial and test conditions of Test 1 and 2

	Initial flow velocity (m/s)	Initial water depth (m)	Bed slope ($\times 10^{-3}$)	Simulation time (s)
1	0.400	5.0×10^{-2}	3.56	2400
2	0.419	8.6×10^{-2}	2.25	3000

Fig. 5 presents the water surface and bed elevation results of Test 1 and 2 respectively, based on the conditions listed in Table 1. The results in Fig. 5(a) were run for 2400s and the results in Fig. 5(b) were run for 3000s. The relatively long duration of computation runs in these two tests could critically examine the capability of the proposed model to handle the long-time sediment aggradation process. Apart from the proposed time-varying sediment adaptation length modelled results, the conventional sediment transport computations without the time-varying approach are also presented to compare with the measurements. Both results in Figs. 5(a) and 5(b) show that the proposed time-varying sediment adaptation length model simulated the sediment aggradation experiments with better agreement. This is particularly true at the channel entrance within 5m from the upstream side, where the local flow conditions changed more quickly, and the time-varying approach showed a very satisfactory agreement with the experimental data while the non time-varying approach produced relatively larger errors. This better agreement further proved the ability of the proposed time-varying approach to simulate long period sediment aggradation in flows.

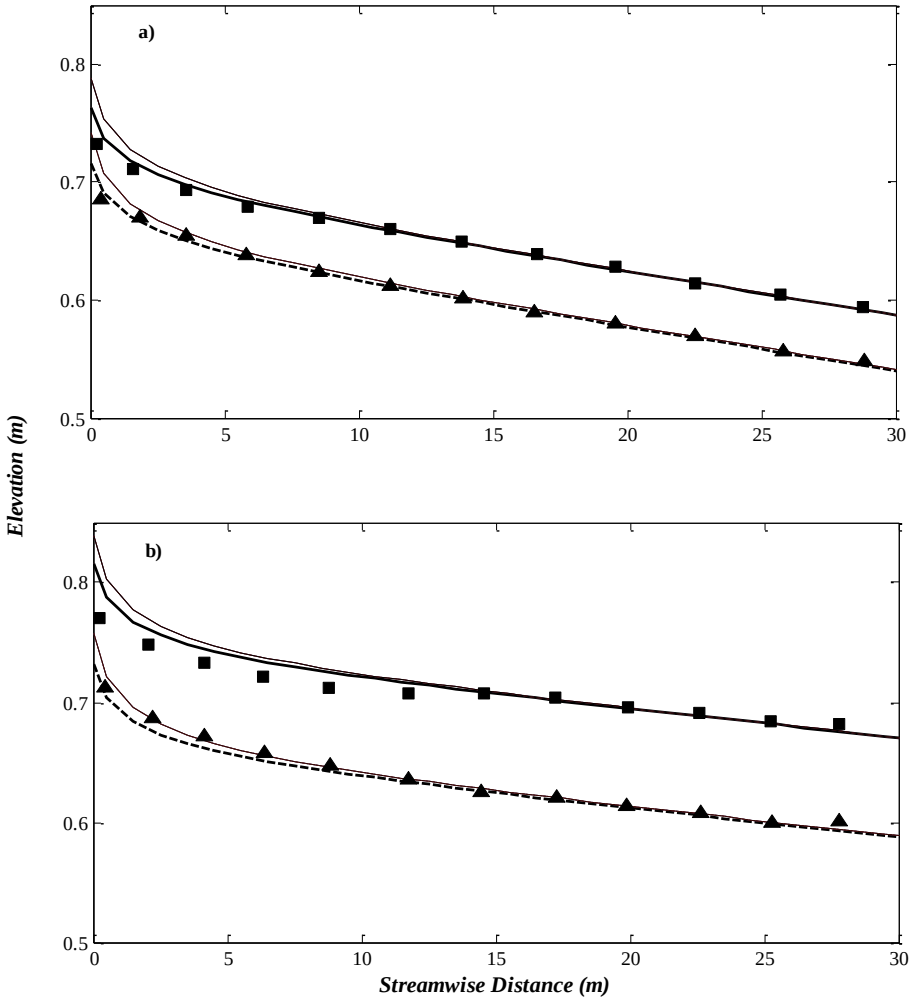

Fig. 5 Water and bed profiles in a) Test 1 and b) Test 2 in Table 1 – simulated water level with T.V.S.A.L.A. (thick solid line), simulated bed level with T.V.S.A.L.A. (thick dashed line), simulated water level without T.V.S.A.L.A. (thin solid line), simulated bed level without T.V.S.A.L.A. (thin dashed line), measured water level (squares) and measured bed level (triangles)

6 Conclusions

In this study, a 2D shallow water Finite Volume (FV) numerical model was applied to analyse the shallow flows with sediment transport. The sediment function added into the model was improved by using a time-varying concept to represent the equilibrium sediment adaptation length. This time-varying sediment adaptation length used the amended erosion-deposition ratio at the pre-equilibrium stage to more precisely represent any rapidly bed changing flows. The proposed model was applied to three separate flow tests. In the first test, a dam break flow over a movable bed was used to calibrate the proposed model. The calibrated model reproduced agreeing results with the experimental measurements

in its water and bed elevation predictions as compared with other models in the literature. The proposed model has also well-captured the enlargement process of the scour hole created by the dam break flow, during which the sediment phase exchanges occurred intensely. In the second test of a highly concentrated flow in a wide alluvial channel, the water and bed elevations were analysed. The comparison with experimental measurements from the literature indicated that the proposed model was capable to predict the highly eroded sediment transport, except for some deposition effects in the channel mid-section, which was believed to be caused by the secondary current. The third test of the sediment aggradation flow also illustrated the efficiency and accuracy of the proposed model to predict flow and sediment evolutions in long period of time. Throughout all three test cases in this study, the proposed model, which was calibrated for the fast scour-hole developing flow application of dam-break sediment transport flow, was also proven to represent the rapid bed change and the steady sediment aggradation flow conditions well.

Acknowledgements

The authors acknowledge the support of the National Natural Science Foundation of China NSFC (Grant Number 20101311246), Major State Basic Research Development Program (973 program) of China (Grant Number 2013CB036402) and Open Fund of the State Key Laboratory of Hydraulics and Mountain River Engineering, Sichuan University of China (Grant Number SKLH-OF-1103). Besides, author Jaan Hui Pu would like to thank Prof. Simon Tait at University of Sheffield for his guidance during the Ph.D study.

References

Armanini A., and Di Silvio G. 1988, A one-dimensional model for the transport of sediment mixture in non-equilibrium conditions. J. Hydraulic Res., Vol. 26, No. 3, pp. 275–292.

Bell R. G., and Sutherland A. J. 1983, Non-equilibrium bed load transport by steady flows. J. Hydraulic Eng., Vol. 109, No. 3, pp. 353–367.

Brufau P., Garcia-Navarro P., Ghilardi P., Natale L., and Savi F. 2000, 1D mathematical modelling of debris flow. J. Hydraulic Res., Vol. 38, No. 6, pp. 435-446.

Cao Z., Pender G., Wallis S., and Carling P. 2004, Computational dam-break hydraulics over erodible sediment bed. J. Hydraulic Eng., Vol. 130, No. 7, pp. 689-703.

Cao Z., Li Y., and Yue Z. 2007, Multiple time scales of alluvial rivers carrying suspended sediment and their implications for mathematical modeling. Adv. Water Resour., Vol. 30, No. 4, pp. 715-729.

Cao Z., Hu P., and Pender G. 2011, Multiple time scales of fluvial processes with bed load sediment and implications for mathematical modeling. J. Hydraulic Eng., Vol. 137, No. 3, pp. 267-276.

Capart H., and Young D. L. 1998, Formation of a jump by the dam-break wave over a granular bed. J. Fluid Mech., Vol. 372, pp. 165-187.

Chen S. C., Peng S. H., and Capart H. 2007, Two-layer shallow water computation of mud flow intrusions into quiescent water. J. Hydraulic Res., Vol. 46, No. 1, pp. 21-34.

Chen R. D., Liu X. N., Cao S. Y., and Guo Z. X. 2011, Numerical simulation of deposit in confluence zone of debris flow and mainstream. Sci. China Tech. Sci., Vol. 54, No. 10, pp. 2618-2628.

Fang H. W. 2003, Case studies of three-dimensional numerical simulation for total sediment transport. Int. J. Sediment Res., Vol. 18, No. 2, pp. 158–165.

Fang H. W., and Wang G. Q. 2000, Three-dimensional mathematical model of suspended-sediment transport. J. Hydraulic Eng., Vol. 126, No. 8, pp. 578-592.

Fang H. W., He G. J., and Wang L. X. 2010, Influence of vertical resolution and nonequilibrium model on three-dimensional calculations of flow and sediment transport. J. Hydraulic Eng., Vol. 136, No. 2, pp. 122-128.

Ferreira R., and Leal J. 1998, 1D mathematical modelling of the instantaneous dam-break flood wave over mobile bed: application of TVD and flux-splitting schemes. Proc. European Concerted Action on Dam-Break Modelling, pp. 175–222. Munich, Germany.

Galappatti G., and Vreugdenhil C. B. 1985, A depth-integrated model for suspended sediment transport. J. Hydraulic Res., Vol. 23, No. 4, pp. 359–377.

Garcia-Martinez R., Espinoza R., Valera E., and Gonzalez M. 2006, An explicit two-dimensional finite element model to simulate short- and long-term bed evolution in alluvial rivers. J. Hydraulic Res., Vol. 44, No. 6, pp. 755-766.

Hu K., Mingham C. G., and Causon D. M. 2006, A mesh patching method for finite volume modelling of shallow water flow. Int. J. Num. Meth. Fluids, Vol. 50, No. 12, pp. 1381-1404.

Huai W. X., Wang Z. W., Qian Z. D., and Han Y. Q. 2011, Numerical simulation of sandy bed erosion by 2D vertical jet. Sci. China Tech. Sci., Vol. 54, No. 12, pp. 3265-3274.

Lin B. N. 1984, Current study of unsteady transport of sediment in China. Proc. Japan-China Bilateral Seminar on River Hydraulics and Engineering Experiences, Tokyo-Kyoto-Saporo, Japan, pp. 337–342.

Lin P. Z., and Wang D. C. 2006, Numerical modelling of 3D stratified free-surface flows: a case study of sediment dumping. Int. J. Num. Meth. Fluids, Vol. 50, No. 12, pp. 1425-1444.

Lin P. Z., Wu Y. N., Bai J. L., and Lin Q. H. 2011, A numerical study of dam-break flow and sediment transport from a quake lake. J. Earthq. Tsunami, Vol. 5, No. 5, pp. 401-428.

Liu C., and Shen Y.-M. 2010, A three dimensional k-ε-A_p model for water-sediment movement. Int. J. Sediment Res., Vol. 25, No. 1, pp. 17-27.

Mingham C. G., and Causon D. M. 2000, Calculation of unsteady bore diffraction using a high resolution finite volume method. J. Hydraulic Res., Vol. 38, No. 1, pp. 49-56.

Nakagawa H., and Tsujimoto T. 1980, Sand bed instability due to bed load motion. J. Hydraulic Div., Vol. 106, No. 12, pp. 2029–2051.

Needham D. J., and Hey R. D. 1991, On nonlinear simple waves in alluvial river flows: a theory for sediment bores. Philos. Trans. Roy. Soc. Lond. A – Math. Phys. Eng. Sci., Vol. 334, No. 1633, pp. 25-53.

Nezu I., and Nakagawa H. 1993, Turbulent Open-Channel Flows (IAHR Monograph). A. A. Balkema, Rotterdam, the Netherlands.

Phillips B. C., and Sutherland A. J. 1989, Temporal lag effect in bed load sediment transport. J. Hydraulic Res., Vol. 28, No. 1, pp. 5–23.

Pu J. H., Cheng N. S., Tan S. K., and Shao S. 2012, Source term treatment of SWEs using surface gradient upwind method. J. Hydraulic Res., Vol.50, No. 2, pp. 145-153.

Rahuel J. L., Holly F. M., Chollet J. P., Belleudy P. J., and Yang G. 1989, Modeling of riverbed evolution for bedload sediment mixtures. J. Hydraulic Eng., Vol. 115, No. 11, pp. 1521–1542.

Singh A. K., Kothyari U. C., and Ranga Raju K. G. 2004, Rapidly varying transient flows in alluvial rivers. J. Hydraulic Res., Vol. 42, No. 5, pp. 473-486.

Soni J. P., Garde R. J., and Ranga Raju K. G. 1980, Aggradation in streams due to overloading. J. Hydraulic Eng., Vol. 106, No. 1, pp. 117-132.

Spasojevic M., and Holly F. M. Jr. 1990, 2-D bed evolution in natural watercourses – New simulation approach. J. Waterway, Port, Coastal and Ocean Eng., Vol. 116, No. 4, pp. 425–443.

Toro E. F. 1999, Riemann Solvers and Numerical Methods for Fluid Dynamics – A Practical Introduction. 2nd ed. Spring-Verlag Berlin Heidelberg.

Valiani A., and Caleffi V. 2001, Dam break modeling for sediment laden flows. Proc. 2001 Int. Symp. Environmental Hydraulics, pp. 1-6. Arizona, USA.

Wren D., Kuhnle R., and Chambers J. 2005, Measurement of suspended-sediment concentration and particle size in laboratory flumes. Proc. Sediment Monitoring Instrument and Analysis Research Workshop, pp. 1-8. Flagstaff, Arizona, USA.

Wu W. 2007, Computational River Dynamics. 1st ed. Taylor and Francis Group London.

Wu W., Rodi W., and Wenka T. 2000, 3D numerical modeling of flow and sediment transport in open channels. J. Hydraulic Eng., Vol. 126, No. 1, pp. 4–15.

Wu W., Vieira D. A., and Wang S. S. Y. 2004, One-dimensional numerical model for nonuniform sediment transport under unsteady flows in channel networks. J. Hydraulic Eng., Vol. 130, No. 9, pp. 914-923.

Wu W., and Wang S. S. Y. 2007, One-dimensional modeling of dam-break flow over movable beds. J. Hydraulic Eng., Vol. 133, No. 1, pp. 48-58.

Xia J., Lin B., Falconer R. A., and Wang G. 2010, Modeling dam-break flows over mobile beds using a 2D coupled approach. Adv. Water Resour., Vol. 33., No. 2, pp. 171-183.

Yang C. T., and Greimann B. P. 1999, Dambreak unsteady flow and sediment transport. Proc. European Concerted Action on Dam-Break Modelling, pp. 327–365. Zaragoza, Spain.

Zhou J., and Lin B. 1998, One-dimensional mathematical model for suspended sediment by lateral integration. J. Hydraulic Eng., Vol. 124, No. 7, pp. 712-717.